Available *online* at: http://ajeeet.ft.unand.ac.id/

Andalas Journal of Electrical and Electronic Engineering Technology

ISSN 2777-0079

Analysis Comparison of PSMEID With Preview for Controlling Shock Vibration of UAV's Landing Gear System

Darmawan[1,2], Lovelyson[1], Meifal Rusli[1], Rahmadi Kurnia[2], Amirul Lutfi[2]

[1] *Department of Mechanical Engineering, Universitas Andalas, Padang, Indonesia*
[2] *Department of Electrical Engineering, Universitas Andalas, Padang, Indonesia*

ARTICLE INFORMATION

Received: October 7, 2024
Revised: November 4, 2024
Revised: November 27, 2024
Available online: December 6, 2024

KEYWORDS

Acceleration amplitude, Velocity amplitude, Spring constant (KPS), Sprung mass

CORRESPONDENCE

E-mail: lovelyson@eng.unand.ac.id

A B S T R A C T

Semi-active dampers reduce the effects of shock vibrations because they can operate at specific vibration frequencies at a lower cost than more complex active dampers. PSMEID is one of the alternative methods developed in the semi-active damping system. PSMEID has been developed by adapting it by adding a PSMEID active time prediction system when an impact occurs. This research attempts to compare two types of PSMEID with active time prediction, where the position of each model offered has a different PSMEID mass position when applied to the landing gear damper of an Unmanned Aerial Vehicle (UAV). This comparison aims to give the user a choice among these optimal models suitable for use in multiple conditions. When simulated using the same parameter values, the PSMEID placed on the unsprung mass can reduce acceleration amplitude by up to 6.6 percent when the landing gear is dropped at 0.15 meters from the ground. The model that places the PSMEID on the sprung mass can help reduce the velocity amplitude up to 8.8 percent when dropped at a height of 0.05 meters, and the spring constant value of the PSMEID (KPS) is 1600 N/m. All these simulations show that the PSMEID should be activated just before the landing gear hits the runway surface ($T_B < T_L$).

INTRODUCTION

Vibration isolation is critical, particularly in sensitive equipment and structure applications. The primary goal of vibration isolation is to minimize the transmission of vibrational energy from a source to a sensitive receiver, thereby protecting it from potential damage or performance degradation. Various techniques have been developed to achieve effective vibration isolation, which can be broadly categorized into passive, active, and semi-active systems.

Passive vibration isolation systems utilize materials and structures that dampen vibrations without external control. These systems often rely on the properties of materials such as rubber or elastomers, which can absorb and dissipate vibrational energy. For instance, laminated rubber-steel bearings have been employed since the 1960s to protect structures from ground-borne vibrations, such as those produced by underground trains [1]. Recent studies have demonstrated the effectiveness of passive techniques in improving the vibration performance of office floors using laminated elastomeric bearings [2]. Additionally, quasi-zero-stiffness isolators have been shown to effectively isolate low-frequency vibrations, making them suitable for applications like vehicle seating [3].

On the other hand, active vibration isolation systems employ sensors and actuators to counteract vibrations actively. These systems can adapt to changing conditions and provide superior performance, especially in low-frequency ranges where passive systems may struggle. For example, a study highlighted the development of an active torsional vibration damper for vehicle powertrains, which significantly mitigated torsional vibrations that arise from modern internal combustion engine technologies [4]. Furthermore, active systems have been successfully implemented in micro-vibration isolation platforms, which effectively utilize external forces to control vibrational energy [5]. The integration of advanced control methodologies, such as Kalman filtering, has also been explored to enhance the performance of active vibration isolation systems [6].

Semi-active vibration isolation systems represent a hybrid approach, combining elements of both passive and active systems. These systems adjust their properties in response to external stimuli, allowing for improved adaptability and performance. Research has shown that semi-active systems, such as tunable damping mechanisms, can significantly reduce vibrations in vehicle suspension systems [7]. Moreover, using harmful stiffness devices in conjunction with enhanced damping has been shown to improve the efficacy of vibration isolation across a broader frequency range [8]. This adaptability makes

https://doi.org/10.25077ajeeet.v5i1.135

semi-active systems appealing for applications requiring robust performance under varying operational conditions.
In conclusion, vibration isolation encompasses various techniques with advantages and limitations. Passive systems provide a straightforward and reliable solution for many applications, while active and semi-active systems offer enhanced performance and adaptability. Ongoing research continues to refine these technologies, further exploring innovative materials and control strategies to improve vibration isolation effectiveness across various engineering domains.

Passive Damper

The design and implementation of passive dampers for isolating shock vibrations in aircraft landing gear systems is a critical area of research, particularly regarding enhancing the safety and comfort of aircraft operations. While traditionally effective, passive dampers face limitations in adaptability to varying landing conditions.

Recent studies have explored various methodologies to optimize the performance of these systems. One significant aspect of passive dampers is their absorbing impact energy during landing. The shock absorber is a fundamental component of landing gear, designed to mitigate the forces exerted on the aircraft during touchdown. Research indicates that the performance of these shock absorbers can be influenced by factors such as the design of the metering pin and the characteristics of the damping materials used [9][10][11]. For instance, Nkemdirim discusses the linear quadratic Gaussian control of landing gear, emphasizing the importance of optimizing damper behavior to improve overall landing performance [12]. It is corroborated by findings from Yıldız, who notes that semi-active systems, which can adjust their damping properties, outperform passive systems in vibration mitigation [13].

Moreover, the dynamics of landing gear systems are complex and require careful modeling to predict their behavior under various conditions. Studies by Sivakumar et al. have utilized nonlinear mathematical models to analyze the impact of runway conditions on landing gear performance, highlighting the necessity of adaptive control strategies to enhance vibration isolation [14]. The integration of advanced materials, such as magnetorheological fluids, has also been proposed to improve the damping characteristics of landing gear systems, allowing for a more responsive approach to shock absorption [15][16][17].

In addition to the mechanical aspects, the design of passive dampers must consider the overall structural integrity of the landing gear. Research by Son emphasizes the importance of dimension variations in landing gear, which can significantly affect static strength and dynamic response [18]. It is particularly relevant when considering the cumulative effects of repeated landings on the materials used in shock absorbers, as highlighted by the work of Shi, who examined the optimization of passive shock absorbers [19].

Furthermore, the advancements in computational modeling techniques have facilitated a deeper understanding of the interactions between various landing gear system components. For example, finite element analysis has been instrumental in simulating the dynamic behavior of landing gear under different loading conditions, allowing for the identification of potential failure modes and the optimization of design parameters [20]. This approach is essential for ensuring that passive dampers can effectively isolate vibrations without compromising the structural integrity of the landing gear. In conclusion, while passive dampers remain a vital component of landing gear systems, ongoing research is focused on enhancing their performance through innovative design, material selection, and advanced modeling techniques. Integrating adaptive control strategies and exploring new damping materials are promising avenues for improving the shock isolation capabilities of landing gear, ultimately contributing to safer and more comfortable aircraft operations.

Active Damper

The current research on active dampers for isolating shock vibrations in aircraft landing gear has seen significant advancements, particularly in integrating magnetorheological (MR) dampers and other active control technologies [21]. These innovations aim to enhance the performance of landing gear systems by effectively managing the dynamic loads experienced during landing and taxiing.

Active and semi-active control methods have emerged as viable solutions for improving the shock absorption capabilities of the landing gear. For instance, Vencatasawmy and Xue highlight the advantages of actively controlled landing gears, which can adapt to varying conditions and significantly improve buffer performance compared to passive systems [10]. The incorporation of MR dampers allows for real-time adjustments to damping characteristics, providing precise control over landing dynamics and enhancing shock absorption [23]. This adaptability is crucial during the critical landing phases, where the landing gear must effectively mitigate impact forces and vibrations [24]. Research by Kang et al. emphasizes the modeling and control of landing gear systems equipped with MR dampers, demonstrating that these systems can achieve better shock attenuation through sophisticated control strategies [22][24]. The use of MR fluids in dampers enables rapid changes in damping force, which can be tailored to specific landing conditions, thereby improving the overall stability and comfort of the aircraft during landing [25][26]. Furthermore, studies have shown that intelligent control algorithms, such as neural networks, can optimize the performance of MR dampers, enhancing their effectiveness in various landing scenarios [27][28].

In addition to MR dampers, other active control technologies are being explored. For example, integrating feedback loops and pumps in active suspension systems has been proposed to dynamically adjust the shock absorption characteristics of landing gear [29]. This approach not only improves energy dissipation during landing but also contributes to the overall structural integrity of the aircraft by reducing the transmission of vibrations to the fuselage [15][30].

Moreover, developing robust control systems for active landing gear has been a focal point of recent research. Studies have demonstrated that advanced control strategies, such as Linear Quadratic Gaussian (LQG) control, can effectively manage the dynamic responses of landing gear systems, ensuring optimal performance under varying operational conditions [12][31].

 https://doi.org/10.25077/ajeeet.v5i1.135

Implementing these control systems is critical for enhancing the reliability and safety of landing gear, particularly in complex landing environments where traditional passive systems may fall short. In conclusion, integrating active dampers, particularly those utilizing MR technology, represents a significant advancement in the design and functionality of aircraft landing gear systems. These innovations improve shock absorption and vibration isolation and enhance aircraft operations' safety and comfort during landing and taxiing.

Semi-Active Damper

Recent advancements in semi-active dampers for isolating shock vibrations in aircraft landing gear have shown significant promise in enhancing landing performance and stability. Semi-active dampers, particularly those employing magnetorheological (MR) fluids, have emerged as a leading technology due to their ability to adjust damping characteristics in real-time based on control inputs. This adaptability allows for improved energy dissipation without compromising system stability, making them suitable for dynamic landing conditions [15][32][33].

The implementation of semi-active control systems in landing gear has been extensively studied. For instance, Yıldız highlights the effectiveness of semi-active dampers in varying damping forces according to control inputs, which is crucial during landing maneuvers [32]. Nkemdirim further elaborates on the operational dynamics of semi-active systems, contrasting them with passive and active systems and emphasizing their role in enhancing the overall performance of landing gear [12]. MR dampers are particularly noted for their fast response to magnetic fields, allowing for rapid adjustments to damping forces, which is vital during the transient phases of landing [15][33].

The design and optimization of these systems have also been a research topic. The research investigated neural network-based intelligent control strategies to regulate MR dampers with the ability to enhance adaptability and performance for different landing conditions [34]. Additionally, Han et al. focused on the effect of magnetic core properties under various conditions of MR damper-based landing gear systems. They emphasized the performance in terms of material through experiments [33]. Nonetheless, hybrid actuators will significantly improve the performance of semi-active landing gear systems when combined with advanced control algorithms like Linear Quadratic Gaussian (LQG) control [12][35].

Moreover, applying semi-active dampers extends beyond traditional aircraft to uncrewed aerial vehicles (UAVs), where Son et al. proposed innovative designs to mitigate shock vibrations during landing [18]. This adaptability across different platforms highlights the versatility of semi-active damping technologies in modern aerospace engineering.
In conclusion, the research on semi-active dampers for isolating shock vibrations in landing gear systems emphasizes their critical role in enhancing landing performance through real-time adaptability and advanced control strategies. The ongoing exploration of MR fluids and intelligent control systems continues to pave the way for innovations that promise to improve aircraft safety and operational efficiency.

PSMEID as a Semi-active Damper

While it is feasible to employ semi-active dampers with variable or negative stiffness in UAV landing gear, secondary advantages are presented alongside the variability of damping. These new semi-active devices can significantly reduce transmitted vibrations over a wide frequency range by adaptively tuning the natural frequency of the landing system [36].

The research on the parameters available for vibration control through the design of damper systems has reached the next stage, in which passive systems are considered by other means, such as momentum changes described by Momentum Exchange Impact Damper (MEID). The MEID, in turn, is divided into two types: Passive-MEID (PMEID) and active-MEID (AMEID). PMEID is a passive damper system that uses momentum change where the kinetic energy generated when growing on the central mass will be transferred to a mass that acts as passive damping [37]. AMEID replaces the damper system with hydraulic, pneumatic, and magnetorheological damper actuators. As per Gregory, the Newton cradle is the base method both use. Figure 1 — Ball Collision Simulation[38]: is to use the changing momentum of collision between the first ball and the second ball equivalent with the amount of momentum when the second ball gives direction to the third had gym then crosses the third already gave half no more than that which should give it so that position will remain fixed.

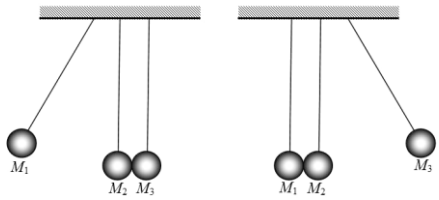

Figure 1. Newton Caddle

The combination of the above two methods, PMEID and AMEID, led to the development of Pre-Staining Spring-MEID (PSMEID). This second ball is the M_P (or central mass) in the PSMEID process, as illustrated by Figure 2 [39]. The mass of the first object is thought to be Body force (FW), and The mass of the third object (M_C) is taken as Spring force after stretching due to the initial spring strain applied on it; this property is called Pre-Staining Spring.

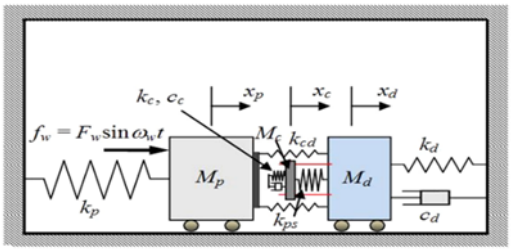

Figure 2. Introduce the PSMEID model

During impact, PSMEID allows the primary energy to be amplified to be more pronounced even in tuning and, more importantly, in reducing the maximal velocity of the drone and transmission forces during landing. The following is a simple model of a UAV landing gear with PSMEID, as illustrated in

Figure 3: when the landing gear hits the runway, a time gap exists between PSMEID mass and central mass, enough for the PSMEID mass to start motion.

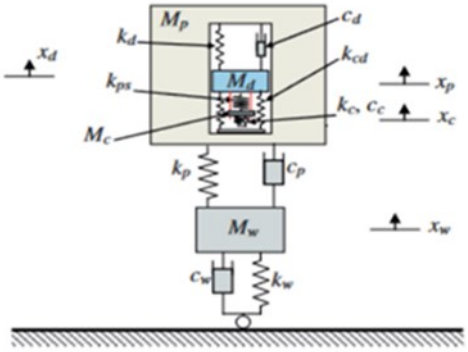

Figure 3. PSMEID on UAV's Landing Gear

Using this model, the following study will invent a method to decide when the perfect moment to turn on the PSMEID is and whether it should be turned on before or after landing gear touches down the runway. Continuing with the previous work on active dampers, the model needs a sensor mechanism to estimate the time of impact [41]. A preview method for an active damping system was developed by the study [42] (Figure 4). This approach places an optical sensor between the external and central mass, which can determine the movement in a contactless fashion. The actuating element is composed of a damper mass secured to the push-rod. The rod is preloaded by the coil springs' initial deflection, corresponding to the preload at an initial load. This is continuously actuated by hydraulic force, which deflects the coil spring. Rod is initially lying in some small free space from the central mass. Accordingly, when the external mass strikes the central mass, an impulsive force is opposed externally, and neutrals, kinetic energy transfer to the rod is due to the release of a strained spring [42].

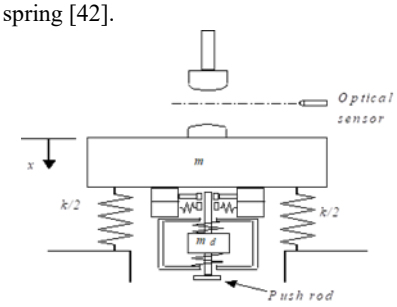

Figure 4. Damper system with Preview

PHYSICS AND MATHEMATICAL MODEL

To evaluate the performance of the PSMEID applied to the damper of UAV's landing gear system model, a comparative study was carried out for two models: model 1 is the model that places the PSMEID on the central mass. In contrast, model 2 is the model that places the PSMEID on the wheel mass.

Model 1 (PSMEID on Sprung)

This model places the PSMEID mass (contact mass) inside the central mass or what is later referred to as the sprung mass, as shown in Figure 5.

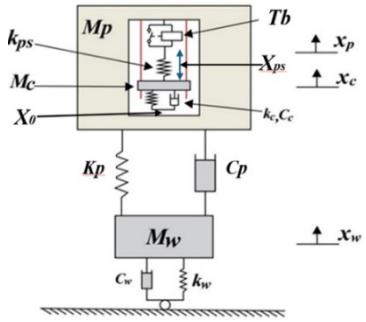

Figure 5. Simulation model of PSMEID on Sprung with Preview

The dynamics of the landing gear of an uncrewed aircraft consist of the main mass, denoted as M_p, supported by the landing gear system. The main spring K_p and damper C_P model the interaction between the main mass and the landing gear system. The landing gear system includes the wheel mass M_w, spring K_W, and wheel damper C_w. The PSMEID damper consists of the contact mass M_C, connected to M_p through pre-strain springs k_{ps}, contact spring k_c, and contact damper C_c.

Assuming that $x_w > x_c > x_p$, using Newton's Second Law, the mathematical equation in Figure 3 can be expressed as:

$$M_p\ddot{x}_p + M_p g - F_{pw} + F_{ps} - F_s = 0 \quad (1)$$
$$M_c\ddot{x}_c + M_c g - F_{cp} - F_s + F_{ps} = 0 \quad (2)$$
$$M_w\ddot{x}_w + M_w g + F_{pw} + F_w = 0 \quad (3)$$

F_w is the impulsive force generated when the landing gear contacts the ground. The unmanned aircraft system is assumed to descend with an initial zero speed.

$$F_w = \begin{cases} c_w\dot{x}_w + k_w x_w, & if\ x_w > 0 \\ 0, & if\ x_w = 0 \end{cases} \quad (4)$$

The relationship between mass M_c and M_p is modeled using k_c and c_c, resulting in the contact force obtained from the motion of the stiffness k_c and damping c_c. The contact force is expressed as:

$$F_{cp} = \begin{cases} C_c(\dot{x}_p - \dot{x}_c) + k_c(x_p - x_0 - x_c), & if\ (x_w - x_0 - x_c) > 0 \\ 0, & if\ (x_w - x_0 - x_c) = 0 \end{cases} \quad (5)$$

The counterforce F_s between M_p and M_c to balance the pre-stress force. The counterforce becomes zero after the main mass collides with the contact spring. This relationship can be expressed as:

$$F_s = \begin{cases} k_{ps}\, x_{ps}, & t = t_b \\ 0, & t \neq t_b \end{cases} \quad (6)$$

Where t is the time measured when the main mass is dropped freely until the landing wheels touch the runway, while t_b is the variable representing the delay time for activating the PSMEID system.

 https://doi.org/10.25077/ajeeet.v5i1.135

The initial gap x_0 in equation (5) is introduced to obtain the optimum condition for transferring momentum from M_p and M_w. The pre-strain spring is added between M_p and M_c to enhance the momentum exchange from the main mass to the contact mass. The pre-strain force value is controlled by adjusting the initial deflection of the pre-stretched spring, as shown in Figure 3.2. The pre-strain force F_{ps} acting between M_p and M_c can be written as:

$$F_{ps} = k_{ps}(x_{ps} + x_c - x_p) \quad (7)$$

F_{pw} is the force of interaction through the spring k_p and damper c_p. This force is calculated from the relative motion between mass M_p and M_w:

$$F_{pw} = c_p(\dot{x}_w - \dot{x}_p) + k_p(x_w - x_p) \quad (8)$$

Model 2 (PSMEID on Unsprung)

The landing gear system with PSMEID on Unsprung is modeled using a combination of several masses, as shown in Figure 6. There are three masses, namely $\boldsymbol{M_p}$, which is the main mass of the drone equipped with a mass wheel; $\boldsymbol{M_w}$, and $\boldsymbol{M_c}$, which is the PSMEID mass that provides momentum to the wheel mass. A spring constant is expressed in $\boldsymbol{K_p}$ and $\boldsymbol{C_p}$ as a damping constant between the main and the wheel mass. The wheel mass has a spring constant $\boldsymbol{K_w}$ and a damping constant $\boldsymbol{C_w}$—Mass $\boldsymbol{M_w}$, which functions to connect to $\boldsymbol{M_p}$ with spring constant $\boldsymbol{K_p}$ and damping $\boldsymbol{C_p}$. Meanwhile, the $\boldsymbol{K_{ps}}$ spring will push the $\boldsymbol{M_w}$ mass to give the opposite momentum.

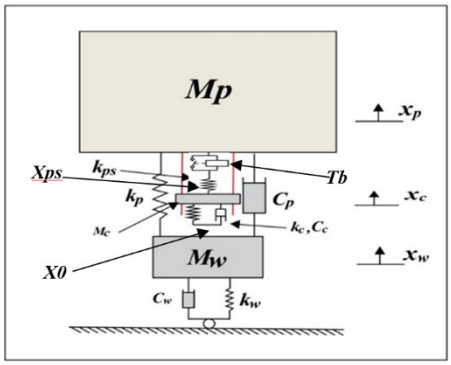

Figure 6. Simulation model of PSMEID on Unsprung with Preview

From the physical model designed as in Figure 5, we can obtain a mathematical model that will be used as the basis for making the simulation using MATLAB/Simulink software.

It is assumed that by using Newton's Law II, the mathematical equation in Figure 5 can be expressed by:

$$M_p\ddot{x}_p + M_p g - F_{pw} + F_{ps} = 0 \quad (9)$$

$$M_c\ddot{x}_c + M_c g - F_{cp} - F_s + F_{ps} = 0 \quad (10)$$

$$M_w\ddot{x}_w + M_w g + F_{pw} + F_w + F_{cp} - F_s + F_{ps} = 0 \quad (11)$$

F_w is the impulsive force generated when the wheel is in contact with the ground. The drone system is assumed to descend with an initial velocity of zero.

$$more\ significantmore\ significant F_w = \begin{cases} c_w\dot{x}_w + k_w x_w, & if\ x_w > 0 \\ 0, & if\ x_w = 0 \end{cases} \quad (12)$$

The contact condition between main mass $\boldsymbol{M_p}$ and wheel mass $\boldsymbol{M_w}$ is modeled using a spring constant $\boldsymbol{K_c}$ and a damper constant $\boldsymbol{C_c}$, resulting in a contact force obtained from the strain motions $\boldsymbol{K_c}$ and $\boldsymbol{C_c}$. The contact force is expressed by:

$$F_{cp} = \begin{cases} C_c(\dot{x}_p - \dot{x}_c) + k_c(x_p - x_0 - x_c), if\ (x_w - x_0 - x_c) > 0 \\ 0, \qquad if\ (x_w - x_0 - x_c) = 0 \end{cases} \quad (13)$$

The counteracting force $\boldsymbol{F_s}$ is between $\boldsymbol{M_p}$ and $\boldsymbol{M_c}$ to balance the pre-strain force. The counteracting force becomes zero once the main mass collides with the contact spring. This relationship can be expressed as:

$$F_s = \begin{cases} K_{ps}\, x_{ps}, & T = Tb \\ 0, & T \neq Tb \end{cases} \quad (14)$$

Where $\boldsymbol{T}$ is the calculated time when the landing gear starts to be dropped in free-fall motion from a certain height, while $\boldsymbol{T_b}$ *is the* time variable of the PSMEID system activation, the initial gap in equation (3.5) is introduced to obtain the optimum condition for transferring momentum from $\boldsymbol{M_p}$ and $\boldsymbol{M_c}$. A pre-stretched spring is added between $\boldsymbol{M_p}$ and $\boldsymbol{M_c}$ to enhance the momentum exchange from the main mass to the contact mass. The value of the pre-stretch force is controlled by adjusting the initial deflection of the pre-stretch spring, as shown in Figure 4.1. The pre-strain force $\boldsymbol{F_{ps}}$ acting between $\boldsymbol{M_p}$ and $\boldsymbol{M_c}$ and can be written as:

$$F_{ps} = k_{ps}(x_{ps} + x_c - x_p) \quad (15)$$

$\boldsymbol{F_{pw}}$ is the interaction force through spring kp and *damper* cp. This force is calculated from the relative motion between masses $\boldsymbol{M_p}$ and $\boldsymbol{M_w}$:

$$F_{pw} = c_p(\dot{x}_w - \dot{x}_p) + k_p(x_w - x_p) \quad (16)$$

Table 1. Simulation Parameters

Parameter	Value	Unit
Main Mass $\boldsymbol{M_P}$	2	Kg
Main Spring Stiffness $\boldsymbol{K_p}$	20000	N/m
Main Damper $\boldsymbol{C_p}$	989,95	Ns/m
The First Contact Mass $\boldsymbol{M_c}$	0,125-0.250	Kg
The First Contact Spring Stiffness $\boldsymbol{k_c}$	2000	N/m
The first Contact Damper $\boldsymbol{C_c}$	9000	Ns/m
The First Pre-strain Spring Stiffness $\boldsymbol{K_{ps}}$	80-1600	N/m
Wheel Mass $\boldsymbol{M_w}$	0.35	Kg
Wheel Spring Stiffness $\boldsymbol{k_w}$	40000	N/m
Wheel Damper $\boldsymbol{C_w}$	392	Ns/m
The First Pre-straining Spring Displacement $\boldsymbol{X_{ps}}$	0.01-01	m
gravity g	9,8	m/s^2
height of fall $\boldsymbol{h}$	0.05,0.1,0.15	m
Gap $\boldsymbol{X_0}$	0,0005	m
Landing Time $\boldsymbol{T_L}$	0.101,0.143,0.175	sec
Active Time of the First PSMEID $\boldsymbol{T_B}$	-	sec

RESULTS AND DISCUSSION

Effect of T_B

This simulation shows the primary mass acceleration response difference for the first model that places the active time prediction PSMEID system on the main mass (Sprung Mass). The second model places the active time prediction PSMEID system on the wheel mass (Unsprung Mass). In this simulation, the active time determined is the best in each model. This simulation is carried out by dropping the UAV landing gear from three variations of the fall height of 0.05, 0.10, and 0.15 meters. Each drop height will result in different landing times (T_L) of 0.101, 0.143, and 0.175 seconds, respectively. Other parameters used are based on Table 1.

Height of fall 0.05 metres

In this condition, the simulation was performed by dropping the landing gear from a distance of 0.05 meters from the runway surface. Thus, it can be determined that the landing time (T_L) is 0.101 seconds. This simulation's mass is 2 Kg, and the PSMEID (M_C) mass is 0.250 kg. Figure 7 shows that the lowest acceleration amplitude occurs in the first model with an active time of 0.096 seconds ($T_B<T_L$), with the maximum acceleration occurring at 63.66 m/s^2. The second model's best active time is 0.1 seconds ($T_B<T_L$), with an acceleration of 64.34 m/s^2. With the above results, it can be seen for a fall height of 0.05 meters, the placement of PSMEID on the wheel mass can reduce the maximum acceleration better than the others.

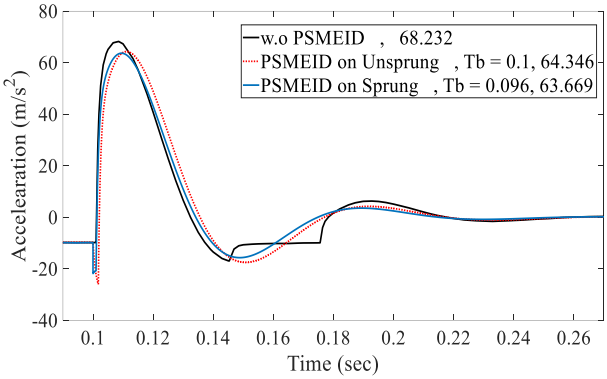

Figure 7. Acceleration response for the best active time at a fall height of 0.05 for model 1 and model 2

Height of fall 0.10 metres

Simulations at a landing wheel fall height of 0.10 meters showed that the first model, PSMEID, decreased the acceleration amplitude by 3.6 percent or from 98.75 m/s^2 to 95.17 m/s^2, as shown in Figure 8. For the second model, PSMEID reduced the acceleration amplitude by 4.4 percent. This indicates a fall height of 0.10 meters PSMEID. The second model effectively isolates the vibration acceleration for the same other parameters. For PSMEID active time, both models used are the same, namely 0.14 seconds ($T_B<T_L$), or PSMEID will be activated before the landing gear reaches the runway surface.

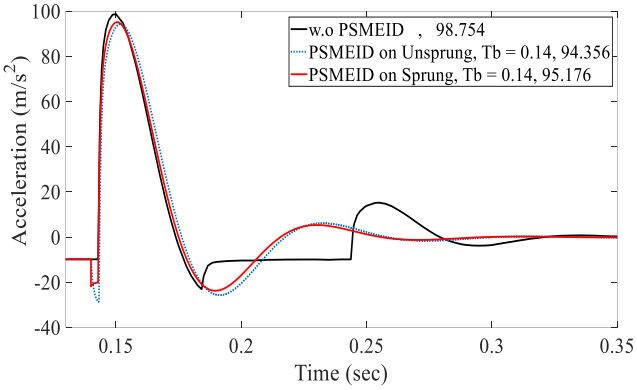

Figure 8. Acceleration response for the best active time at a fall height of 0.10 for model 1 and model 2

Height of fall 0.15 metres

For the height of the landing gear falling from a distance of 0.15 meters, the landing time (T_L) is 0.175 seconds using a simple calculation of free fall motion. The graph in Figure 9 shows that the PSMEID on the unsprung (second model) can reduce the acceleration amplitude by 6.06 percent, with the most optimal PSMEID active time at 0.173 seconds after the landing gear starts to drop ($T_B<T_L$). Meanwhile, the first model can reduce 1.75 percent of the acceleration amplitude reduction.

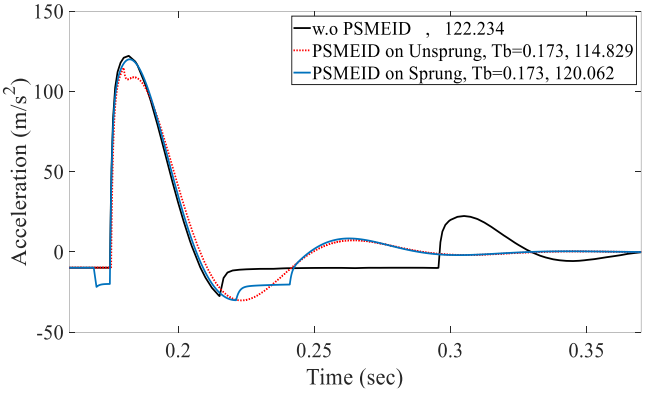

Figure 9. Acceleration response for the best active time at a fall height of 0.15 for model 1 and model 2

Variation of K_{PS} and X_{PS} on System's Performance

The spring constant of the PSMEID (K_{PS}) and the PSMEID spring press distance (X_{PS}) are two parameters that significantly affect the performance of the landing gear damper. The greater the K_{PS} value, the greater the potential energy value of the PSMEID system, as well as the spring deflection of the PSMEID, which is linearly proportional to the potential energy when applying force to the unsprung mass and sprung mass in the landing gear system.

Effect of K_{PS}

The landing gear drop height of 0.05 meters with the variation of spring constant (K_{PS}) can be seen in Figure 10. the K_{PS} for PSMEID model 1 decreases acceleration amplitude as the K_{PS} value increases. In contrast, for PSMEID model 2, the K_{PS} value of 1200 N/m contributes the best reduction in acceleration amplitude. For the PSMEID activation time, model 1 is activated 0.096 seconds after the landing gear is released from a height of 0.05 meters ($T_B<T_L$), while model 2, the PSMEID, will activate at 0.1 seconds.

 https://doi.org/10.25077/ajeeet.v5i1.135

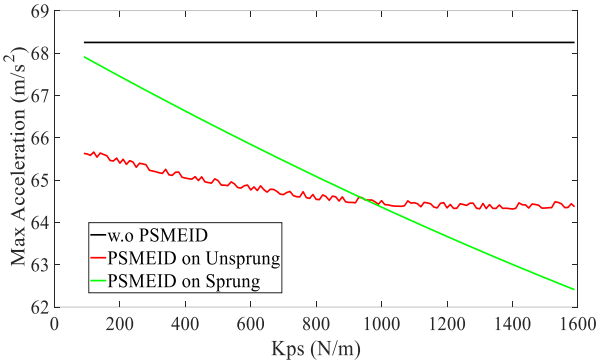

Figure 10. Comparison of the effect of $\mathbf{K_{PS}}$ value on amplitude acceleration of two PSMEID models for 0.05 meters landing gear drop simulation

For the landing gear drop height of 0.1 meters from the runway surface, the effect of the K_{PS} on both models can be seen in the graph shown in Figure 11. When the K_{PS} variation is tested on the first model, it can be seen that the higher the K_{PS} value, the higher the decrease in velocity amplitude, while for the second model, the K_{PS} makes the maximum contribution to the reduction in acceleration amplitude when the K_{PS} value is 1100 N/m, or it can be said that this phenomenon is the same as the simulation at the height of 0.05 meters. All variations of the K_{PS} value use the best active time for a fall height of 0.10 meters, which is 0.14 seconds (T_B<T_L) in both model 1 and model 2.

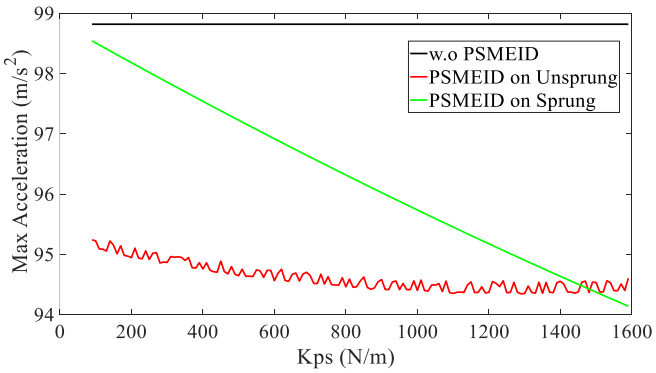

Figure 11. Comparison of the effect of $\mathbf{K_{PS}}$ value on amplitude acceleration of two PSMEID models for 0.10 meters landing gear drop simulation

In the simulation of the landing gear drop height of 0.15 meters, the K_{PS} value in model 2 shows a significant influence tendency when the K_{PS} value gets bigger, far exceeding the influence of K_{PS} in model 1, as shown in Figure 12. All these variations of the K_{PS} value use the best active time for a drop height of 0.15 meters, which is 0.173 seconds (T_B<T_L) in both model 1 and model 2.

Effect of X_{PS}

Theoretically, when the X_{PS} is greater, the kinetic energy stored in a spring will be more incredible. On the other hand, it should be noted that the PSMEID's mass not only provides momentum once during the first impact but also possibly that the following momentum is relatively minor, which may affect the vibration in the landing gear. The parameters used for this X_{PS} variation simulation are the same as for the KPS variation, especially for the PSMEID uptime.

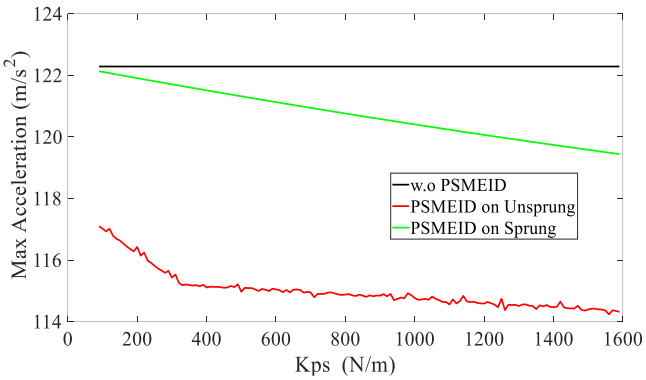

Figure 12. Comparison of the effect of $\mathbf{K_{PS}}$ value on amplitude acceleration of two PSMEID models for 0.15 meters landing gear drop simulation

Simulations by varying the X_{PS} when the landing gear is dropped at a height of 0.05 meters are shown in Figure 13. The response graph shows that for model 2 (PSMEID on unsprung), the X_{PS} will optimally reduce the acceleration amplitude when it is pulled 0.02 meters from its balance point. As for model 1, the decrease in acceleration amplitude will be proportional to the increase in X_{PS}, and determining this variable will have certain limitations when applied because the spring length used has a limited value.

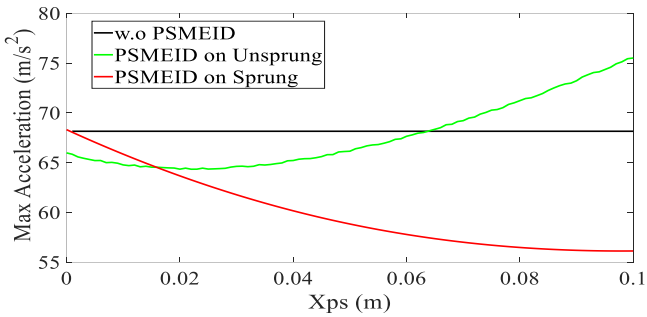

Figure 13. Comparison of the effect of $\mathbf{X_{PS}}$ value on amplitude acceleration of two PSMEID models for 0.05 meters landing gear drop simulation

For the landing gear fall height of 0.1 meters, the acceleration amplitude with X_{PS} variation is shown in the graph in Figure 14. X_{PS} in Model 1 contributes significantly to the decrease of acceleration amplitude when the spring compression distance is enlarged; in other words, this phenomenon is the same as when simulating the fall height of 0.05 meters. As for model 2, the optimal X_{PS} can reduce the acceleration amplitude to 0.02 meters, the same as the simulation for the landing gear drop height of 0.05 meters.

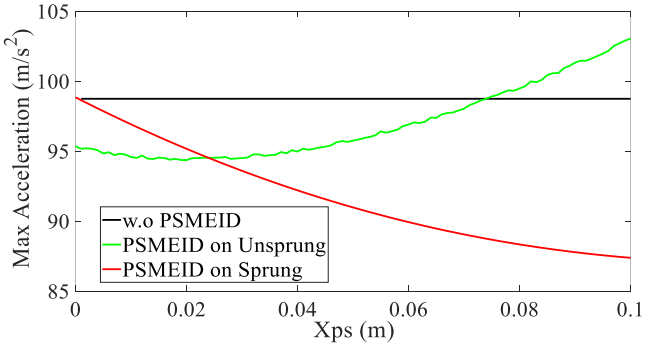

Figure 13. Comparison of the effect of $\mathbf{X_{PS}}$ value on amplitude acceleration of two PSMEID models for 0.10 meters landing gear drop simulation

A different phenomenon occurs for the fall height of 0.15 meters, compared to the two previous fall heights of 0.05 and 0.1 meters. Both models show a decrease in acceleration amplitude when X_{PS} is enlarged, but PSMEID model 2 shows a more significant reduction in acceleration amplitude than PSMEID model 1, as shown in Figure 14.

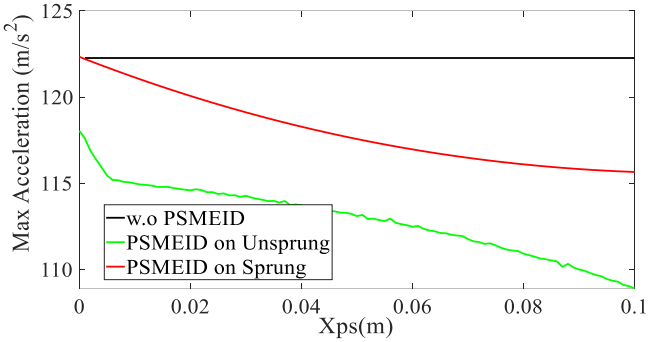

Figure 13. Comparison of the effect of X_{PS} value on amplitude acceleration of two PSMEID models for 0.15 meters landing gear drop simulation

CONCLUSIONS

From the two PSMEID models that have been developed, it can be concluded that each model has its advantages and disadvantages. Both PSMEID models with time prediction will have an optimal effect on reducing the acceleration of shock vibrations on the landing gear damper when activated before the landing gear reaches the runway surface ($T_B<T_L$), expressly limited to the main mass of 2 Kg. Model 2 PSMEID tends to make a more significant contribution to the field of model 1 when applied to the number of parameters, but on the other hand, if specific parameter values are used, such as K_{PS} and X_{PS}, the decrease in acceleration amplitude will be more significant.

REFERENCES

[1]. Orfeo, A., Tubaldi, E., Muhr, A., & Losanno, D. (2022). Mechanical behavior of rubber bearings with low shape factor. Engineering Structures, 266, 114532. https://doi.org/10.1016/j.engstruct.2022.114532.

[2]. Ghafar, N., Rahimi, M., & Goh, L. (2022). Human comfort assessment of vibration behavior of office floors: before and after strengthening using the laminated elastomeric bearing. International Journal of Sustainable Construction Engineering Technology, 13(2). https://doi.org/10.30880/ijscet.2022.13.02.025

[3]. Abuabiah, M., Dabbas, Y., Herzallah, L., Alsurakji, I., Assad, M., & Plapper, P. (2022). Analytical study on the low-frequency vibrations isolation system for vehicle seats using quasi-zero-stiffness isolator. Applied Sciences, 12(5), 2418. https://doi.org/10.3390/app12052418.

[4]. Yüceşan, A. and Muğan, A. (2021). Development and control of an active torsional vibration damper for vehicle powertrains. Proceedings of the Institution of Mechanical Engineers Part K Journal of Multi-Body Dynamics, 235(3), 452-464. https://doi.org/10.1177/14644193211019943.

[5]. Pan, G., Liu, D., & Xiao, Y. (2016). Simulation and experiment study on six-degrees-of-freedom active micro-vibration isolation platform.. https://doi.org/10.2991/msota-16.2016.30

[6]. Shahadat, M., Mizuno, T., Takasaki, M., Rashid, F., & Ishino, Y. (2021). Vibration isolation system with Kalman filter estimated acceleration feedback: an approach of negative stiffness control. Journal of Sensors, 2021(1). https://doi.org/10.1155/2021/961646.

[7]. Zheng, H., Liang, P., & Xiang, Y. (2015). Tunable stiffness and damping isolator based on modified skyhook control method.. https://doi.org/10.2991/icmeis-15.2015.56

[8]. Nagarajaiah, S., Zou, K., & Herkal, S. (2022). Reduction of transmissibility and increased efficacy of vibration isolation using negative stiffness device with enhanced damping. Structural Control and Health Monitoring, 29(11). https://doi.org/10.1002/stc.3081.

[9]. Ding, Y., Wei, X., Nie, H., & Li, Y. (2018). Discharge coefficient calculation method of landing gear shock absorber and its influence on drop dynamics. Journal of Vibroengineering, 20(7), 2550-2562. https://doi.org/10.21595/jve.2018.19049.

[10]. Vencatasawmy, D. and Xue, C. (2020). Research on landing gear metering pin and analysis of its impact on the buffer performance. International Journal of Engineering Research And, V9(07). https://doi.org/10.17577/ijertv9is070229.

[11]. Shi, F., Dean, W., & Suyama, T. (2019). Single-objective optimization of passive shock absorber for landing gear. American Journal of Mechanical Engineering, 7(3), 107-115. https://doi.org/10.12691/ajme-7-3-1.

[12]. Nkemdirim, C. (2023). Linear quadratic Gaussian control of a 6-of aircraft landing gear. Energies, 16(19), 6902. https://doi.org/10.3390/en16196902.

[13]. Yıldız, A. (2024). Semi-active control implementation in aircraft landing gear systems using a hardware-in-the-loop test bench. Engineering Research Express, 6(3), 035529. https://doi.org/10.1088/2631-8695/ad68c3.

[14]. Sivakumar, S., Selvakumaran, T., & Sanjay, B. (2021). The random runway effect on the landing of an aircraft with active landing gears was investigated using the nonlinear mathematical model. Journal of Vibroengineering, 23(8), 1785-1799. https://doi.org/10.21595/jve.2021.21915.

[15]. Viet, L. and Hwang, J. (2019). A semi-active controller for an aircraft landing gear equipped with a magnetorheological damper. Applied Mechanics and Materials, 894, 29-33. https://doi.org/10.4028/www.scientific.net/amm.894.29.

[16]. Han, C., Kim, B., Kang, B., & Choi, S. (2019). Effects of magnetic core parameters on landing stability and efficiency of magnetorheological damper-based landing gear system. Journal of Intelligent Material Systems and Structures, 31(2), 198-208. https://doi.org/10.1177/1045389x19862639.

[17]. Kang, B., Jo, B., Kim, B., Hwang, J., & Choi, S. (2023). Linear and nonlinear models for drop simulation of an aircraft landing gear system with MR dampers. Actuators, 12(7), 287. https://doi.org/10.3390/act12070287.

[18]. Son, L. (2023). The effect of landing gear dimension variation on uncrewed aerial vehicle's static strength and dynamic response (UAV). International Journal of Automotive and Mechanical Engineering, 20(3), 10745-10757. https://doi.org/10.15282/ijame.20.3.2023.16.0830.

[19]. Shi, F. (2019). Multi-objective optimization of passive shock absorber for landing gear. American Journal of Mechanical Engineering, 7(2), 79-86. https://doi.org/10.12691/ajme-7-2-4.

[20]. Lin, Q. (2024). Structural strength analysis and optimization of commercial aircraft nose landing gear under towing taxi-out conditions using finite element simulation and modal testing. Aerospace, 11(5), 414. https://doi.org/10.3390/aerospace11050414.

[21]. Luong, Q., Jang, D., & Hwang, J. (2020). Robust adaptive control for an aircraft landing gear equipped with a magnetorheological damper. Applied Sciences, 10(4), 1459. https://doi.org/10.3390/app10041459.

[22]. Kang, B., Jo, B., Kim, B., Hwang, J., & Choi, S. (2023). Linear and nonlinear models for drop simulation of an aircraft landing gear system with MR dampers. Actuators, 12(7), 287. https://doi.org/10.3390/act12070287.

[23]. Kang, B., Yoon, J., Kim, G., & Choi, S. (2020). Landing efficiency control of six degrees of freedom aircraft model with magnetorheological dampers: part 2—control simulation. Journal of Intelligent Material Systems and Structures, 32(12), 1303-1315. https://doi.org/10.1177/1045389x20942593.

[24]. Kang, B. (2024). Design, structure analysis, and shock control of aircraft landing gear system with Mr. Damper. Smart Materials and Structures, 33(5), 055049. https://doi.org/10.1088/1361-665x/ad3e53.

[25]. Han, C., Kim, B., Kang, B., & Choi, S. (2019). Effects of magnetic core parameters on landing stability and efficiency of magnetorheological damper-based landing gear system. Journal of Intelligent Material Systems and Structures, 31(2), 198-208. https://doi.org/10.1177/1045389x19862639.

[26]. Yoon, J., Kang, B., Kim, D., & Choi, S. (2020). New control logic based on mechanical energy conservation for aircraft landing gear system with magnetorheological dampers. Smart Materials and Structures, 29(8), 084003. https://doi.org/10.1088/1361-665x/ab9e11.

[27]. Luong, Q., Jo, B., Hwang, J., & Jang, D. (2021). A supervised neural network control for magnetorheological damper in an aircraft landing gear. Applied Sciences, 12(1), 400. https://doi.org/10.3390/app12010400.

[28]. Le, Q. (2023). Intelligent control and a model predictive control for a single landing gear equipped with a magnetorheological damper. Aerospace, 10(11), 951. https://doi.org/10.3390/aerospace10110951.

[29]. Ahmad, M., Shah, S., Shams, T., Javed, A., & Rizvi, S. (2020). Comprehensive design of an oleo-pneumatic nose landing gear strut. Proceedings of the Institution of Mechanical Engineers Part G Journal of Aerospace Engineering, 235(12), 1605-1622. https://doi.org/10.1177/0954410020979378.

[30]. Delebarre, C. (2019). Smart aircraft landing gear: the mechatronic approach. Journal Electrical and Electronic Engineering, 7(6), 170. https://doi.org/10.11648/j.jeee.20190706.16.

[31]. Pirooz, M., Mirmahdi, S., & Khoogar, A. (2021). Robust force and displacement control of an active landing gear for vibration reduction at touchdown and during taxiing. Sn Applied Sciences, 3(4). https://doi.org/10.1007/s42452-021-04320-1.

[32]. Yıldız, A. (2024). Semi-active control implementation in aircraft landing gear systems using hardware-in-the-loop test bench. Engineering Research Express, 6(3), 035529. https://doi.org/10.1088/2631-8695/ad68c3.

[33]. Han, C., Kim, B., Kang, B., & Choi, S. (2019). Effects of magnetic core parameters on landing stability and efficiency of magnetorheological damper-based landing gear system. Journal of Intelligent Material Systems and Structures, 31(2), 198-208. https://doi.org/10.1177/1045389x19862639.

[34]. Luong, Q., Jang, D., & Hwang, J. (2020). Intelligent control based on a neural network for aircraft landing gear with a magnetorheological damper in different landing scenarios. Applied Sciences, 10(17), 5962. https://doi.org/10.3390/app10175962.

[35]. Luong, Q., Jang, D., & Hwang, J. (2020). Robust adaptive control for an aircraft landing gear equipped with a magnetorheological damper. Applied Sciences, 10(4), 1459. https://doi.org/10.3390/app10041459.

[36]. Abdalaziz, M., Vatandoost, H., Sedaghati, R., & Rakheja, S. (2023, February 1). Design and experimental characterization of a bypass magnetorheological damper featuring variable stiffness and damping. IOP Publishing, 32(3), 035011-035011. https://doi.org/10.1088/1361-665x/acb474.

[37]. Darmawan, L Son, Mulyadi Bur, Nurmansyah," Experimental Studies of Application Passive Momentum Exchange Impact Damper (PMEID) on UAV'S Landing Gear", IOP Conf. Series: Materials Science and Engineering, doi:10.1088/1757-899X/1041/1/012065.

[38]. L. Son, M. Bur, and M. Rusli, "A new concept for UAV Landing Gear shock vibration control using pre-straining spring momentum exchange impact Peredam," JVC/Journal Vib. Control, vol. 24, no. 8, pp. 1455–1468, 2018, doi: 10.1177/1077546316661470.

[39]. L. Son, M. Bur, M. Rusli, H. Matsuhisa, K. Yamada, and H. Utsuno, "Fundamental study of momentum exchange impact damper using pre-straining spring mechanism," Int. J. Acoust. Vib., vol. 22, no. 4, pp. 422–430, 2017, doi: 10.20855/ijav.2017.22.4487.

[40]. Ghasemalizadeh, O., Taheri, S., Singh, A., & Goryca, J. (2014, January 1). Semi-active Suspension Control using Modern Methodology: Comprehensive Comparison Study. Cornell University. https://doi.org/10.48550/arxiv.1411.3305.

[41]. Uçan, F., & Pak, M. (2013, April 1). A guidance system for unmanned air vehicles. https://doi.org/10.1109/siu.2013.6531305.

[42]. Tanaka, N., dan Kikushima, Y. 1987, "A Study on the dynamic Peredam with a preview action (1st report, a principle of the dynamic Peredam with a preview action)", J. Jpn. Soc. Mech. Eng.,(in Japanese), Vol. 52 No.484, C(1986), pp.3176-3183.